Mechanisms of time-modulated polarized nano-crystalline diamond growth

Cyril Faure, Lionel Teulé-Gay, Jean-Pierre Manaud, Angeline Poulon-Quintin

Mechanisms of time-modulated polarized nano-crystalline diamond growth

Cyril Faure, Lionel Teulé-Gay, Jean-Pierre Manaud, Angéline Poulon-Quintin

CNRS, Université de Bordeaux, ICMCB, Pessac, France

Abstract

Two bilayer systems (TaN/Mo and ZrN/Mo) have been deposited onto WC–Co cermets in order to limit the cobalt diffusion from this substrate and to promote the diamond nucleation. Mo was the top layer. The diamond CVD coating process includes two steps: 1) Bias Enhance Nucleation (BEN) step for diamond nucleation control, 2) diamond growth step with a time-modulated negative substrate polarization to form nanocrystalline diamond grains (NCD). Original cluster morphology of diamond film was obtained, and patented under the name PyrNCD (for pyramidal NCD). Clusters are multilayered and composed of two diamond layers (resp. grain sizes: about 1 nm and 10 nm) periodically repeated. Thermomechanical computations have been carried out to understand the stress distribution inside the multilayer systems before and after diamond deposition. Computation results demonstrate that the architecture of the system is optimized and the morphology of PyrNCD diamond clusters should not degrade their substrate adhesion. A mechanism for the formation of the diamond layer is proposed for a time-modulated polarized diamond growth process to understand the formation of both the specific morphology and the NCD grains.

Keywords : NCD ; Time-modulated biased diamond ; Multilayer systems ; Carbon diffusion ; Diamond growth mechanism ; Tooling applications

1. Introduction

Composite material machining requires the production of erosion resistive cutting tools coated with ultra-hard materials like diamond. Inability to manufacture effective diamond coated cutting tools is due to technical problems such as delamination during production and to the low fracture toughness of diamond (3–4 $MPa.m^{1/2}$). As a consequence, extensive researches on using diamond as hard coating is developed but faced two main difficulties. First, the strength of purely covalent bonds between carbon atoms prevents them from forming chemical bonding to the substrate material in order to assure the adequate adhesion. Second, for WC–Co cermets, the cobalt metallic binder is well known to catalyze the formation of sp^2 graphitic species [1-2] detrimental for the adhesion of diamond.

To limit the cobalt diffusion close to the interface with diamond, two main methods may be considered:

- Binder removal from the top surface of the cermet substrate using acidic treatments (Caro's acid [3-4], Murakami's reagent [3], [5-7]),

- The use of intermediate layers as cobalt diffusion barrier and controlling the carbon diffusion phenomenon during the diamond deposit [8-15].

The first method is cheap, fast and easily integrated into production chains. It remains the most commonly used in industry. Unfortunately the chemical attack weakens the interface with a debonding of the WC grains leading to a more

brittle area and delamination by grain shedding. As a consequence, this method is not coherent with the principle of using a larger quantity of binder in cutting tools in order to increase their resilience. The intermediate layer method turns out to be an interesting alternative. No additional tool surface preparation is required but unfortunately problems of adhesion subsist. In a previous study [16], we have shown that the use of some metallic interlayers (NbN, TaN and ZrN) of 1 μm thickness can efficiently stop the cobalt diffusion through the surface. The boundaries between the substrate (WC–Co) and these interlayers are partially coherent (metallic bonding) and as a consequence are very strong [17]. However, the diamond nucleation density is generally less important on the metallic carbides and nitrides than on their pure metal form [4].

As a consequence, the design of bilayer systems has been optimized to isolate the cobalt from the diamond and to increase diamond nucleation. The first layer, the metallic nitride coating at the interface with the substrate, acts as a diffusion barrier for the cobalt. It is composed of TaN likely to carburize during diamond deposition or of ZrN thermochemically stable in the CVD conditions used [16], [19]. This layer is then coated with a thin molybdenum [18] layer dedicated to enhance the diamond nucleation density (called here the “diamond nucleation layer”). Some authors have also proposed to use titanium [4], [9], [10-11], but thermochemical computation has shown that the bilayer system TaN–Ti is thermodynamically unstable for diamond CVD range of process temperature [19]. Hence, this work focuses on the TaN–Mo and ZrN–Mo bilayer systems used to enhance the time-modulated polarized diamond growth with a control of cobalt and carbon diffusion phenomena during the diamond formation at the interface and a control of the NCD cluster morphology.

2. Experimental

2.1. Bi-layer system deposition

Substrates were commercially available WC–12% Co square 16 × 16 mm^2 pads and 4 mm thick. They have been sand-blasted under the following conditions: P = 2 bar, t = 15 s. Average surface roughness (measured by a white light confocal profilometer VEECO) equals 380 ± 50 nm and root-mean-square roughness 480 ± 60 nm. Prior to the growth of intermediate layer deposits, ultrasonic cleaning with acetone and then propane-1-ol vapors are used in order to eliminate impurities on the surface. Diffusion barrier and diamond nucleation layer were deposited using a reactive magnetron sputtering Plassys MP700 plant. The temperature of the substrates was fixed at 673 K [16]. The target to substrate distance was set at 70 mm for all deposits to guarantee a uniform layer thickness in respect of a fair deposition rate.

Nitride layers are deposited by reactive sputtering of tantalum (99.98%) and zirconium (99.8%) metallic targets in an argon–nitrogen (Dinal Alphagaz 2, > 99.999%) plasma. Deposition conditions have been optimized in previous works and are presented in Table 1. The ultimate pressure before processing was $1–2 \cdot 10^{-5}$ Pa. Deposition rates are accurately extrapolated from nitride layer thicknesses deposited on silicon wafers. The diamond nucleation layer was obtained from a molybdenum (99.98% Cerac) target sputtered in an ultrapure argon (Dinal Alphagaz 2, > 99.999%) plasma. Moreover, this gas was purified passing through a R.D. Mathis purifier (titanium heated at 1023 K).

Table 1
Reactive sputtering deposition parameters of nitride materials at 673 K.

Sample	Total pressure (Pa)	Partial N_2 pressure (Pa)	N_2 percentage (%)	Power density ($W.cm^{-2}$)	Target voltage (V)	Deposition rate ($nm.min^{-1}$)	Layer thickness (μm)
TaN	0.5	0.05	10	2.3	−160	10.0	1.0
ZrN	0.5	0.03	6	4.0	−280	16.5	1.0
Mo	0.5	–	–	2.3	−190	20.0	0.5

2.2. Diamond deposition

Diamond deposition was carried out using a home-made microwave tubular CVD reactor. The 50 mm quartz tube crosses a waveguide powered by a 2.45 GHz microwave generator that can yield a power of up to 2 kW. A system to apply an independent DC bias to the substrate placed 1 cm above a grounded core anode, has also been added.

Our coating process is a mix between the works reported by Vandenbulcke et al. [20-22], who synthesized diamond deposits using a multiple-step process, and by Q.H. Fan [23] or G. Cabral [24], who used a variable methane concentration during the diamond growth process, named time-modulated CVD (TMCVD). Multilayer diamond coatings on WC–12%Co substrates are synthesized without prior seeding and using a two-step growth process. First, nucleation step was carried out with a high methane concentration (3%) and a BEN (bias enhanced nucleation) at − 200 V [25-29]. Second, a "time-modulated polarized growth step" (TMPGS) is achieved at lower methane concentration (0.8%). It consists of alternating two sequences n-times. The first one is a diamond growth without substrate bias. The second one is assumed to be a secondary diamond nucleation obtained by biasing the substrate at − 200 V. In this work, the duration of this two alternated sequences was fixed to 30 min each. This protocol has been patented (WO/2010/076423, [30]). The CVD deposition conditions are presented in Table 2. The temperature of the sample surface was set at 1150 K (measured with a Raytek biband pyrometer).

Table 2
Bias sequenced MWCVD deposition parameters of PyrNCD film at 1073 K.

	Sequence	CH_4 (%)	Total flow rate (cm^3/min)	Pressure (hPa)	Negative bias (V)	Sequence duration (h)	Total step duration (h)
First nucleation step	Biased	3.0	230	40	−200	0.5	0.5
Polarized modulation growth step	Unbiased	0.8	440	40	0	0.5	6 h 30 min
	Biased	0.8	440	40	−200	0.5	

2.3. Characterization

X-ray diffraction was used to determine the deposited phases thanks to a Philips PW1820 diffractometer with θ/2θ geometry and a Cu K_α radiation proportional detector. Morphology observations were carried out with a SEM Jeol JMS 6360A microscope equipped with a Jeol EDS system. The observation of the diamond layer nanostructure was performed by a Jeol 2200FS TEM equipped with a Jeol EDS/STEM system.

2.4. Thermomechanical computation

Thermomechanical computations – COMSOL Multiphysics® [31] software – have been performed to estimate the thermomechanical stress adaptation depending on the interlayer system and the diamond film morphology: NCD or PyrNCD [30]. The mechanical properties of all the materials used have a wide range of values. For this computation, the retained values presented in Table 3 are mean values issued of bibliography [13], [32-36]. All these values correspond to bulk material properties. As a consequence some difference may occur with the real properties of the materials deposited in thin film. However, the aim of these calculations was to compare qualitatively the strain levels reached in the different multilayer systems.

Table 3
Physical properties of materials (WC–12%Co, TaC, ZrN, Mo_2C, diamond) used for thermomechanical computation [13,32–36,41].

Material	Young modulus (GPa)	Poisson's ratio	Thermal expansion coefficient ($\times 10^{-6}$/K)	Density (g/cm^3)
WC–12%Co	570	0.18	6.2	14.6
TaC	420	0.24	7.2	14.5
ZrN	510	0.19	7.2	7.32
Mo2C	535	0.24	5.1	9.06
Diamond	1000	0.10	1.0	3.51

The significant difference between the thickness of the substrate (4 mm) and the Mo layer (0.0004 mm) has restricted this computation to a 2D approach with a 1 × 1 mm^2 substrate size. The NCD diamond film is modeled by a contiguous cluster set with the same diameter and height (5 µm, Fig. 1). This decomposition would allow simulating the strain distribution between the clusters, the entire interface being considered as perfect (i.e. without roughness, without porosity, without material diffusion…). In order to increase the resolution near of the interface with the layer systems, the substrate was decomposed in two parts linked with a perfect bound. The "substrate 1" has a 20 µm thickness and allows refining the mesh near and in the multilayer system.

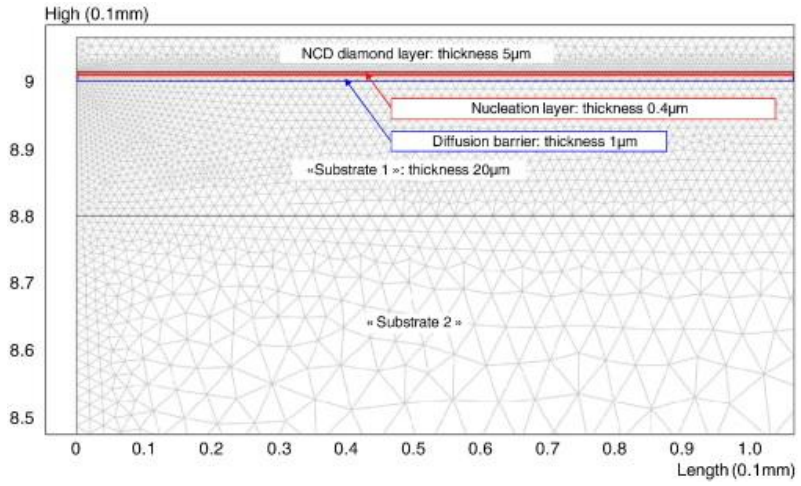

Fig. 1. Mesh presentation of the system for thermomechanical computation.

3. Experimental results

3.1. Coating morphology and microstructure

In a previous work [19], thermomechanical calculation, TEM, XRD and AES analyses have shown that:

- Stoichiometric mono-nitrides MN (M = Ta or Zr) have been synthesized,

- each layer is very dense and continuous,

- no reaction between the different layers occurs before diamond deposition neither at the interface with the substrate,

- no cobalt neither molybdenum diffusion through the diffusion barrier occurs at 400 °C during PVD processes,

- weak cobalt diffusion is noticed through the diffusion barrier during the CVD diamond deposition.

Original pyramidal diamond cluster morphology (Fig. 2) is obtained with NCD deposition condition used in this work. SEM observations validate a continuous diamond layer obtained with a MWCVD process duration of 6 h 30 min. The common spherical morphology usually observed for NCD films is not found here. Each cluster is composed of two parts: a cylindrical base and a conical top (Fig. 2). This pyramidal morphology has been patented under the name PyrNCD [30]. TEM observation proves that each pyrNCD diamond clusters are composed of two kinds of diamond layers corresponding to the unbiased and biased (time-modulated polarized growth step) sequences (Fig. 3). All of these diamond layers are dense with continuous interfaces. HR-TEM observations (not shown here) prove a high difference in diamond grain size according to the biased (about 1.1 ± 0.3 nm) and the unbiased (about 9.0 ± 4.0 µm) sequences. EDS-STEM [19] shows that the Mo nucleation layer is totally sputtered by the ionic bombardment used during the CVD process. Moreover, some cobalt succeeds in diffusing through the diffusion barrier to the interface with the diamond

layer. This cobalt appears under its metallic form or as Co–Mo–C ternary compounds identified by XRD as $Co_6Mo_6C_2$ (PDF 01-080-0339) and Co_2Mo_4C (PDF 01-089-4885). They are localized in a graphite–diamond mixed layer close to the interface with the diffusion barrier [19]. EDS-STEM analyses prove that, to prevent cobalt diffusion from substrate, the ZrN diffusion barrier is more efficient than TaN [30]. The formation of a nanocrystalline diamond layer was confirmed by Raman analyses [19].

Nevertheless, the composition choice for the diffusion barrier affects the final diamond cluster size (Fig. 4). When the ZrN/Mo bilayer system is used, no carburization of the diffusion layer occurs during the CVD process. The diamond cluster size distribution is bimodal (1.5 ± 0.5 µm and 10 ± 5 µm; Fig. 4c). In the instance of the TaN/Mo bilayer system, the surface is covered by PyrNCD clusters with average base diameters smaller than 5 µm (Fig. 4a).

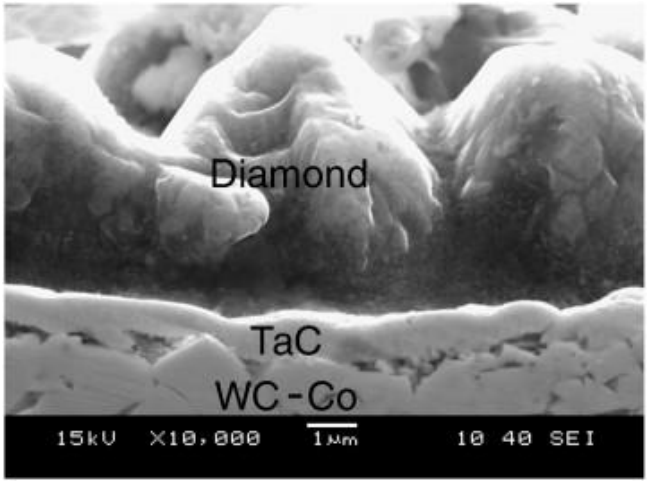

Fig. 2. SEM cross-section picture of PyrNCD on TaN/Mo initial bilayer system: continuous layer and pyramidal diamond cluster morphology.

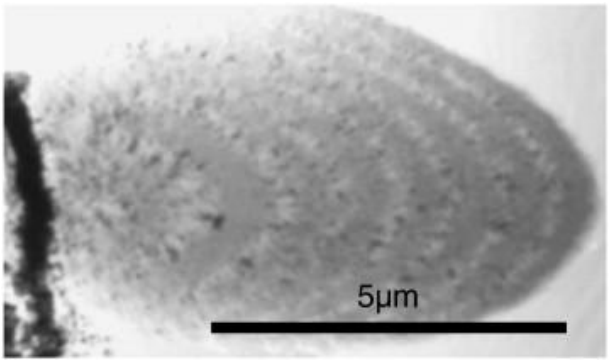

Fig. 3. TEM picture of a PyrNCD cluster composed of layers with different grain sizes depending on bias or unbiased sequences.

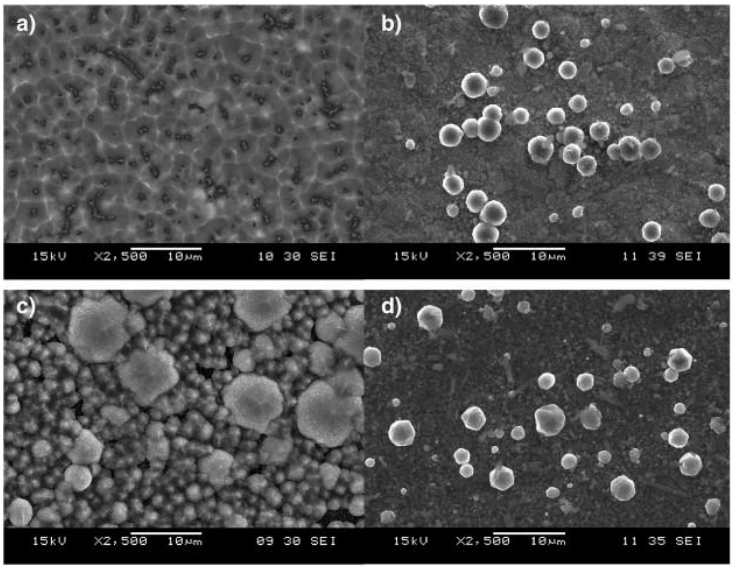

Fig. 4. SEM pictures of PyrNCD layer (top view) deposited on TaN/Mo (a and b) and on ZrN/Mo (c and d) initial bilayer systems after diamond deposition process of 6 h for a) and c) and of 3 h for b) and d).

3.2. Thermomechanical computation

For a NCD film on the initial bilayer system, the use of TaN or ZrN as a cobalt barrier diffusion induces a very slight difference in the stress values and any difference in their distribution. The stresses load progressively from the edge to the center of the substrate. To quantify the effect of the nucleation layer present on the thermomechanical stress distribution, the computation was performed with and without the nucleation layer. Values presented in Table 4 are average values estimated far from the edges. When diamond layer is represented as a continuous layer (named NCD) composed of clusters (square shaped in this case), the removal of the nucleation layer induces a light decrease of the tensile stress value estimated for diffusion layer and no difference for the diamond layer.

Table 4
Intensity of thermomechanical stress according to the cobalt diffusion barrier composition and the diamond cluster morphology (T_{CVD} = 1150 K).

Interlayer system	Nucleation layer	Diamond morphology	Thermal stresses (GPa)			
			Diffusion barrier	Nucleation layer	Diamond	
TaN/Mo	Without	NCD	1.8		−4.8	Zone 1
	With		1.7	1.4	−4.8	Zone 1
	Without	pyrNCD	1.9		−10.0	Zone 3
	With		1.7	1.7	−12.7	Zone 3
ZrN/Mo	Without	NCD	1.9		−4.8	Zone 1
	With		1.8	1.4	−4.8	Zone 1
	Without	pyrNCD	2.0		−10.0	Zone 3
	With		1.8	1.7	−12.7	Zone 3

The stress distribution inside the PyrNCD cluster can be divided into three zones (Fig. 5). The first one corresponds to the cylindrical base of the pyramidal cluster. The tensile stresses in this area are similar to those of the NCD diamond film. The second zone, the conical part of the PyrNCD cluster, is subjected to weak thermomechanical stresses. The third zone is the junction between the two previous ones. This area is subjected to intense compressive stresses (values presented in Table 4). However, this high stress state is located inside the diamond layer at the junction between clusters (Fig. 5). From the perspective of thermomechanical stress distribution based on these results, the original morphology of PyrNCD diamond clusters should not degrade their adherence compared to the NCD morphology. Moreover, the addition of the nucleation layer (subjected to tensile stresses) leads to a reduction of the tensile stress values obtained for the diffusion layer [37]. It should be beneficial to have a more gradual stress distribution from the substrate to the diamond layer.

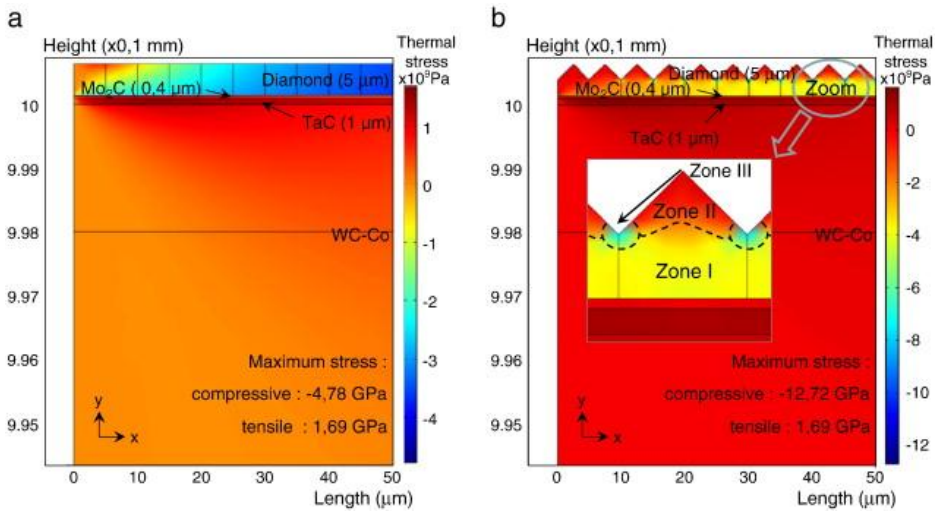

Fig. 5. Thermomechanical stress distributions in a a) NCD and b) PyrNCD diamond coating deposited at 1150 K.

4. Discussion

Diamond cluster size differences depending on the chosen diffusion barrier can be explained by their carbon solubility and carbon diffusion coefficient.

Fig. 6 presents the evolution of the logarithm of the diffusion coefficient Ln(D) as a function of the inverse temperature 1/T for TaC [38], ZrN [39] and Mo_2C [40]. From 1400 K to 3000 K, the diffusion coefficient values for ZrN are always lower than for TaC, itself lower than for Mo_2C.

For both systems, the nucleation layer is composed of molybdenum. During diamond deposition process, the molybdenum layer is carburized in Mo_2C. The carbon diffusion coefficient in Mo_2C is estimated to $4 \cdot 10^{-12}$ cm^2/s at 1150 K (CVD process temperature); an intermediate value compared to the values obtained for others carbides [18]. As a consequence during the process, the formation of numerous diamond nuclei occurs thanks to a high initial nucleation step and the formation of a diamond continuous layer is possible.

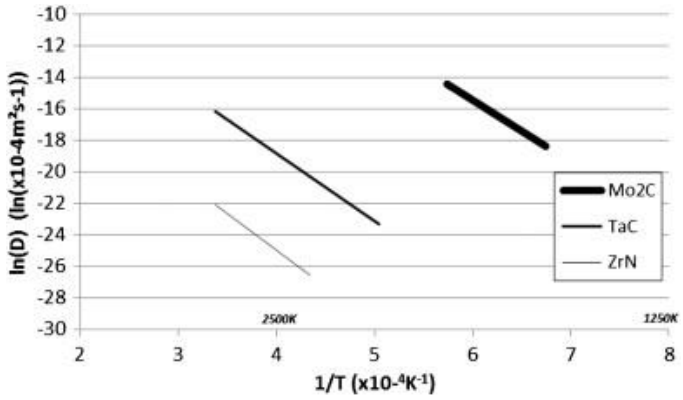

Fig. 6. Diffusion coefficient evolution as a function of temperature for TaC [38], ZrN [39] and Mo_2C [40]: Ln(D) = f(1 / T).

Depending on the diffusion barrier composition, carburization happens (TaN–Mo system) or not (ZrN–Mo system). As observed by Joffreau et al. [18] for single layer systems, nucleation density and final grain sizes depend on the carbon solubility inside the substrate. When the carbon diffusion coefficient is low as for TaC (estimated to $1 \cdot 10^{-17}$ cm^2/s at 1150 K by extrapolation of the curve and announced to be equal to $2 \cdot 10^{-14}$ cm^2/s without temperature details by [18]), a very low solubility of carbon is possible, super-saturated areas are few represented and as a consequence, a low nucleation occurs and large grains of diamond are formed. When the carbon diffusion coefficient is high as for TiC ($1 \cdot 10^{-8}$ cm^2/s, [18]), a very high solubility of carbon is possible, super-saturation areas are numerous and

homogeneously distributed at the surface. Thus a lot of nuclei are formed and small grains of diamond appear. But due to the competition between dissolution and growth, the formation of a continuous diamond layer is difficult. Joffreau and al. [18] have shown that to obtain a satisfactory diamond nucleation density, a compromise has to be done between a high carbon solubility to preserve homogeneous distribution of diamond nucleus and a moderate carbon solubility to preserve diamond nuclei from dissolution.

In our case, an interlayer system composed of a nucleation layer with an intermediate carbon diffusion coefficient (Mo) coated on a diffusion layer composed of either a low coefficient (TaN carburized in TaC, $1 \cdot 10^{-17}$ cm^2/s at 1150 K) or a very low coefficient (stable ZrN until 1150 K, $1 \cdot 10^{-21}$ cm^2/s at 1150 K) is used. During the diamond deposition process, due to the TaC formation, the TaN–Mo system dissolves more carbon than the ZrN–Mo system. Without the use of a bias sequenced CVD process, this carbon solubility difference should explain the homogeneous spatial distribution of diamond nuclei at the beginning of the process for the TaN–Mo system with the carburization of the molybdenum nucleation layer as well as carbon dissolution into the TaN layer to form TaC. As a result at the end of the CVD process, a non-continuous diamond layer should be obtained. Whereas for the ZrN–Mo system, without carburization of the ZrN diffusion layer, the mechanism obtained for molybdenum should prevail over ZrN one. In this case, the carbon solubility in the ZrN–Mo bilayer system could be optimized with the nucleation layer thickness leading to the formation of a continuous diamond layer. In this study, the first step of the CVD process is the nucleation step carried out with a high methane concentration and the use of a bias applied to the substrate. Due to the etching effect, first nuclei are formed on defects produced on the molybdenum layer surface and inside area saturated in carbon. Ionic bombardment can also induce nuclei sputtering at the top surface of the interlayer systems. Depending on the system, the nucleus density can be affected and as a consequence, the cluster distribution can be modified as noticeable Fig. 4 b) for TaN/Mo and Fig. 4 d) for ZrN/Mo. An estimation of the cluster density after 3 h of diamond growth is $1.7 \cdot 10^6$ nucleus/cm^2 for TaN–Mo and $1.3 \cdot 10^6$ nucleus/cm^2 for ZrN–Mo. No continuity of diamond cluster layer is observed but a cluster size difference is already noticeable. The average cluster size after 3 h of diamond growth is 2.5 ± 0.8 μm for TaN–Mo with a maximal of 3.7 μm and a minimal of 1.0 μm and for ZrN–Mo, 1.8 ± 1.0 μm with a maximal of 4.3 μm and a minimal of 0.2 μm. The presence of a lot of small clusters (< 1 μm) is noticeable for ZrN–Mo system whereas cluster sizes are more homogeneous for the TaN–Mo system. To conclude on nucleation, the cluster grain size distributions confirm the influence of the selected bilayer system on the nucleation of diamond grains since the first step of process and its consequences for the evolution of the diamond layer. The bimodal cluster size distribution observed for the ZrN–Mo system as well as the homogeneous distribution of cluster size and the discontinuity of the diamond layer observed for the TaN–Mo, are the consequences of the nucleation process in correlation with the diffusion coefficient of carbon inside the selected materials, the possibility of carburization and the use of a bias.

However, in our case independently of the bilayer system selected, diamond layers are composed of clusters of diamond nano-grains due to the use of a sequenced process (with and without applied bias sequences) which reduces the columnar growth of the diamond grains, their coalescence and favors the secondary nucleation. TEM observations of PyrNCD clusters reveal their multilayer structure (Fig. 3); correlated with the alternatively biased and unbiased sequences. For the unbiased sequences, average grain size is 9 ± 4 nm with the presence of few grains for which diameter reaches 50 nm. For the biased sequences, the diamond grain size is reduced to 1.1 ± 0.3 nm. After the first nucleation step process, a time modulated polarized growth step starts. The diamond multilayer formation mechanism described below is illustrated Fig. 7. First diamond growth without bias occurs. Isolated nuclei on the surface as well as the nano-sized diamond grains localized on the first clusters formed can start growing. For these clusters, graphite is predominantly localized at grain boundaries. The next step is a biased sequence. The ionic bombardment occurs. The exposed surfaces are etched; mainly the graphitic carbon [25], [42] and the grain boundaries [41]. Surface of the diamond grains and grain boundaries of the clusters can act as new nucleation sites. Even if the CH_4 content is reduced (0.8%) during the biased sequences, carbon content in the plasma near the surface may be increased due to both carbon species sputtering possibly giving extra sp^3 species under rich H_2 atmosphere and a very short mean free path – about

3 µm in the CVD reactor with the conditions used – allowing energetic species to deposit again to form diamond. Then an enhanced diamond nucleation can occur. Moreover due to the continuous ionic bombardment, growth of diamond grains is reduced. Then during the following unbiased sequence, diamond nucleation on the cluster surface defects can freely occur and growth of diamond grains located at the cluster periphery starts again. The previously described mechanism is repeated until the end of the sequenced process thus leading to the formation of the multilayer PyrNCD clusters.

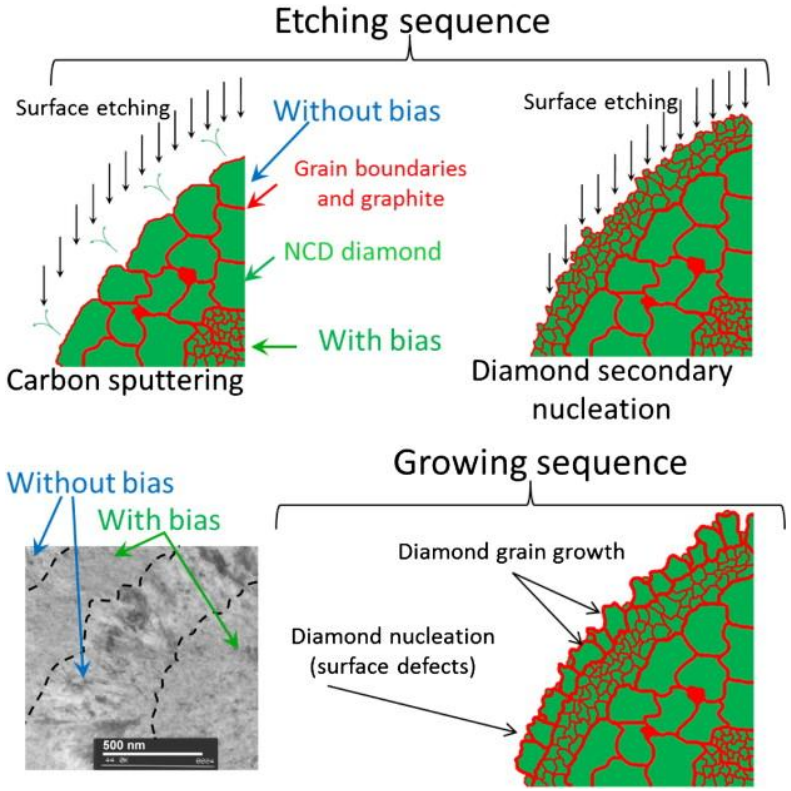

Fig. 7. TEM micrograph and schematic representation of diamond grain growth according each biased/unbiased sequence.

In addition, the previously described mechanism can also explain the pyramidal morphology of the clusters. As noticed Fig. 4, for the TaN–Mo system, the diamond layer composed of a juxtaposition of NCD clusters is less continuous than for the ZrN–Mo system. As previously shown, this observation has to be correlated with the first steps of the nucleation process as a function of the interlayer system used. Since the end of diamond nucleation step, the small clusters (< 1 µm) are spherical (Fig. 8). A first unbiased growth step sequence follows leading to the cluster growth without modification of their spherical morphology. The biased following sequence etches the exposed surfaces with C--H species formation (i.e. the spherical cluster periphery [4]) and begins to induce a conical shape. Then the unbiased sequence starts again etc. The cylindrical base of PyrNCD morphology is then a consequence of the lateral cluster growth and the contact between two cluster neighbors. This mechanism is presented in Fig. 9.

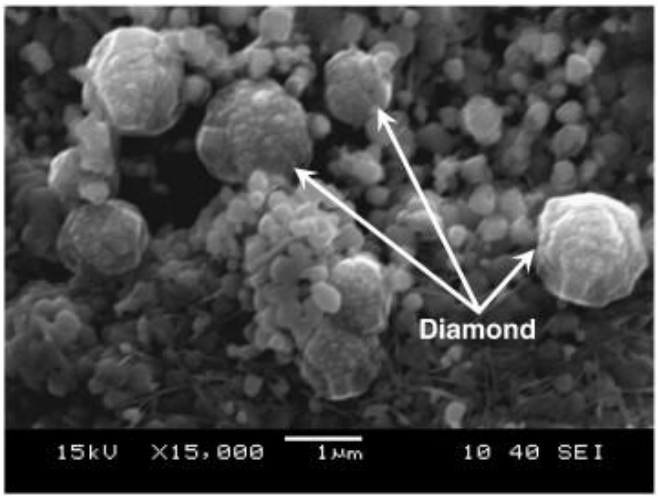

Fig. 8. SEM micrographs of diamond nuclei after the first nucleation step observed on TaN/Mo bilayer system surface.

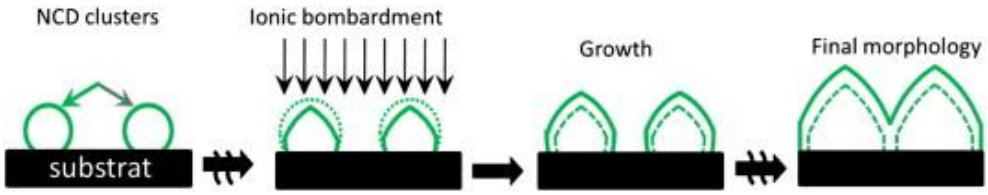

Fig. 9. Schematic representation of PyrNCD diamond cluster growth.

5. Conclusion

The use of interlayer systems allows obtaining continuous diamond films on WC–12%Co substrates without any other surface pretreatment. The biased sequenced MWCVD conditions presented in this paper lead to an atypical diamond cluster morphology which was patented under the name PyrNCD [30]. Moreover, the time-modulated biased growth step leads to the formation of a multilayer diamond cluster with two types of layer showing different grain sizes.

Thermomechanical computations were carried out to understand the stress distribution inside the systems including a substrate, a diffusion layer, a nucleation layer and a diamond layer or not. Computation results demonstrate that the architecture of the system is optimized in terms of interlayer system (material selection and layer thickness) and that the morphology of PyrNCD diamond clusters should not degrade their substrate adhesion.

This work underlines the prominent effect of substrate carbon solubility on the diamond nucleation density as well as the consequences on the clusters size distribution. Using TaN–Mo system, cluster size distribution is homogeneous but the diamond layer is not continuous after 6 h of deposit. For ZrN–Mo system, the cluster size distribution is bimodal and the diamond layer is continuous. The efficiency of the diffusion barrier is a key parameter to control cobalt diffusion, as demonstrated by a previous work [19]. In this study, it is shown that its composition allows modulating carbon diffusion and as a consequence the cluster size distribution of the diamond layer and its continuity.

Two PyrNCD formation models have been elaborated according to the observed scale to explain both the multilayer diamond grain sizes (NCD) and the cluster morphology (PyrNCD morphology). The effect of time-modulated polarized diamond growth allows the formation of a multilayer diamond structure with a control of the final morphology of the diamond cluster.

Acknowledgments

The authors are pleased to thank “Le Conseil Regional d'Aquitaine” for its financial support.

References

1. S. Söderberg, K. Westergren, I. Reineck, P.-E. Ekholm, H. Shahani. Y. Tzeng (Ed.), Applications of Diamond Films and Related Materials: Proceedings of the First International Conference on the Applications of Diamond Films and Related Materials: ADC '91, Auburn, Alabama, U.S.A., August 17–22, 1991, 0444891625, Elsevier (1991), p. 43.
2. J.-A. Montes De Oca – Valero, Thesis, Université de Bordeaux I, N° d'ordre 2582 (2002).
3. K. Mallika, R. Komanduri. Wear, 224 (1999), p. 245.
4. S.K. Sarangi, A. Chattopadhyay, A.K. Chattopadhyay. Int. J. Refract. Met. Hard Mater., 26 (2008), p. 220.
5. H. Sein, W. Ahmed, C. Rego. Diamond Relat. Mater., 11 (2002), p. 731.
6. H. Sein, W. Ahmed, M. Jackson, R. Polini, I. Hassan, M. Amar, C. Rego. Diamond Relat. Mater., 13 (2004), p. 610.
7. R. Polini. Thin Solid Films, 515 (2006), p. 4.
8. I. Endler, A. Leonhardt, H.-J. Scheibe, R. Born. Diamond Relat. Mater., 5 (1996), p. 299.
9. J.M. Lopez, V.G. Babaev, V.V. Khvostov, J.M. Albella. J. Mater. Res., 13 (1998), p. 2841.
10. R. Polini, F. Pighetti Mantini, M. Barletta, R. Valle, F. Casadei. Diamond Relat. Mater., 15 (2006), p. 1284.
11. R. Polini, F.P. Mantini, M. Braic, M. Amar, W. Ahmed, H. Taylor. Thin Solid Films, 494 (1–2) (2006), p. 116.
12. Z. Xu, L. Lev, M. Lukitsch, A. Kumar. Diamond Relat. Mater., 16 (2007), p. 461.
13. Z. Xu, L. Lev, M. Lukitsch, A. Kumar. J. Mater. Res., 22 (4) (2007), p. 1012.
14. G. Cabral, J. Gäbler, J. Lindner, J. Grácio, R. Polini. Diamond Relat. Mater., 17 (2008), p. 1008.
15. R. Polini, M. Barletta. Diamond Relat. Mater., 17 (2008), p. 325.
16. J.P. Manaud, A. Poulon, S. Gomez, Y. Le Petitcorps. Surf. Coat. Technol., 202 (2007), p. 222.
17. H. Holleck. J. Vac. Sci. Technol. A, 4 (6) (1986), p. 2661.
18. P.O. Joffreau, R. Bichler, R. Haubner, B. Lux. J. Ref. Hard Metals, 7 (1988), p. 92.
19. A Poulon-Quintin, C. Faure, L. Teulé-Gay, J.-P. Manaud. Thin Solid Films, 519 (5) (2010), p. 1600.
20. L. Vandenbulcke, D. Rats, M.I. De Barros, R. Benoît, R. Erre, P. Andreazza. Appl. Phys. Lett., 72 (4) (1998), p. 501.
21. M.I. De Barros, D. Rats, L. Vandenbulcke, G. Farges. Diamond Relat. Mater., 8 (1999), p. 1022.
22. M.I. De Barros, L. Vandenbulcke. Diamond Relat. Mater., 9 (2000), p. 1862.
23. Q.H. Fan, N. Ali, Y. Kousar, W. Ahmed, J. Gracio. J. Mater. Res., 17 (2002), p. 1563.
24. G. Cabral, P. Reis, R. Polini, E. Titus, N. Ali, J.P. Davim, J. Grácio. Diamond Relat. Mater., 15 (2006), p. 1753.
25. S. Yugo, T. Kanai, T. Kimura, T. Muto. Appl. Phys. Lett., 58 (10) (1991), p. 1036.
26. W.L. Wang, G. Sánchez, M.C. Polo, R.Q. Zhang, J. Esteve. Appl. Phys. A, 65 (1997), p. 241.
27. I.-H.-H. Choi, P. Weisbecker, S. Barrat, E. Bauer-Grosse. Diamond Relat. Mater., 13 (2004), p. 574.
28. H. Li, M. Gowri, J.J. Schermer, W.J.P. van Enckevort, T. Kacsich, J.J. ter Meulen. Diamond Relat. Mater., 16 (2007), p. 1918.
29. M. Marton, T. Izak, M. Vesely, M. Vojs, M. Michalka, J. Bruncko. Vacuum, 82 (2008), p. 154.
30. J.P. Manaud, A. Poulon-Quintin, L. Teule-Gay, C. Faure, International Patent WO/2010/076423.
31. COMSOL Multiphysics 3.5a, version 3.5.0.6.3, edited 12/03/2008 by COMSOL AB Software.
32. H.O. Pierson. Handbook of Refractory Carbides and Nitrides, Elsevier (1996), p. 17.
33. A.J. McGinnis, T.R. Watkins, K. Jagannadham. Adv. X-ray Anal., 41 (1998), p. 443. (Copyright © JCPDS-International Centre for Diffraction Data 1999).

34. A.J. Perry. Thin Solid Films, 193–194 (Part 1) (1990), p. 463.
35. David R. Lide. Handbook of Chemistry and Physics (85th ed.), 0-8493-0485-7, CRC Press (2004–2005). Section 4, p. 1–168.
36. J.-F. Guillaumond, Thesis, University of Joseph Fourrier Grenoble 1 (2005).
37. A. Poulon-Quintin, C. Faure, L. Teulé-Gay, J.-P. Manaud. Mater. Sci. Forum, 706–709 (2012), p. 2898.
38. R. Resnick, L. Seigle. Trans. Metall. Soc. AIME, 236 (1966), p. 1732.
39. Y.F. Khromov, V.P. Yanchur, V.S. Fiz. Met. Metalloved., 33 (1972), p. 642.
40. A.V. Shovensin, G.V. Scherbedinskii, A.N. Minkevich. Poroshk. Metall., 11 (1966), p. 46.
41. Y.S. Zou, K.L. Ma, W.J. Zhang, Q. Ye, Z.Q. Yao, Y.M. Chong, S.T. Lee. Diamond Relat. Mater., 16 (2007), p. 1208.
42. K. Kobashi. Diamond films—Chemical Vapor Deposition for Oriented and Heteroepitaxial Growth, 0080447236, Elsevier (2005), p. 122.